# Dynamical Downscaling and Loss Modeling for the Reconstruction of Historical Weather Extremes and Their Impacts

## A Severe Foehn Storm in 1925

BY PETER STUCKI, STEFAN BRÖNNIMANN, OLIVIA MARTIUS, CHRISTOPH WELKER, RALPH RICKLI, SILKE DIERER, DAVID N. BRESCH, GILBERT P. COMPO, AND PRASHANT D. SARDESHMUKH

In many parts of the world, intense windstorms represent a major natural hazard, with potential damage to buildings, structures, or forested areas (Jackson et al. 2013; COMET 2014). High-resolution wind and impact data are needed to describe meteorological characteristics and impacts of windstorms. However, such datasets are sparse in Switzerland prior to around 1980, and simulations of storm-related losses mostly cover events from recent decades.

Here, we reconstruct a high-impact foehn storm (definition in AMS 2014) in the Swiss Alps that occurred on 15 February 1925, and we model the associated losses on a local scale. First, we analyze the weather event and the related impact patterns by traditional documentary means. Then, we feed dynamically downscaled wind fields of the Twentieth Century Reanalysis (20CR) ensemble dataset (Compo et al. 2011) into an open-source economic loss model (Bresch 2014) that sweeps this historical windstorm across present-day landscapes and human-built structures. Comparison between the documentary evidence and the model simulation indicates that high-resolution numerical modeling of windstorms and associated losses has the potential to enter an era that has hitherto been the province of environmental historians; and such modeling could extend far beyond the Alps and 15 February 1925.

**AFFILIATIONS:** STUCKI, BRÖNNIMANN, AND WELKER—Oeschger Centre for Climate Change Research and Institute of Geography, University of Bern, Bern, Switzerland; MARTIUS—Oeschger Centre for Climate Change Research, Institute of Geography, and Mobiliar Lab for Natural Risks, University of Bern, Bern, Switzerland; RICKLI—Institute of Geography, University of Bern, and Meteotest, Bern, Switzerland; DIERER—Meteotest, Bern, Switzerland; BRESCH—Swiss Reinsurance Company, Zurich, Switzerland; COMPO AND SARDESHMUKH—Cooperative Institute for Research in Environmental Sciences, University of Colorado, and Earth System Research Laboratory, National Oceanic and Atmospheric Administration, Boulder, Colorado
**CORRESPONDING AUTHOR:** Peter Stucki, Oeschger Centre for Climate Change Research and Institute of Geography, University of Bern, Hallerstrasse 12, Bern, Switzerland
E-mail: peter.stucki@giub.unibe.ch

DOI:10.1175/BAMS-D-14-00041.1



At 0900 LT on that Sunday (0800 UTC), R. Streiff-Becker, a passionate meteorologist, looked through his binoculars toward the Alps from his home in uptown Zurich, Switzerland (see Fig. 1a for locations). He noticed a broadening strip of clear sky that approached the city and contained only a few, fast-traveling clouds. Simultaneously, the Alpine range vanished behind a massive cloud wall. Streiff-Becker spotted several impressive snow plumes over the foothill summits. Shortly thereafter, the forelands and Zurich were caught by surprisingly gusty foehn winds. In his home town of Glarus, which is situated in a north-south-oriented foehn valley, southerly winds had been fierce during the early morning hours, but had already weakened by 1000 LT (0900 UTC). Concurrently, strong drizzle had set in upwind of the Alpine divide, and 24-h precipitation amounts of nearly 200 mm had been observed.

**DOCUMENTARY WEATHER AND LOSS RECONSTRUCTION.** The foehn storm of 15 February 1925 ranks among the most hazardous windstorms in Switzerland since the mid-nineteenth century (Stucki et al. 2014). Substantial documentation is available on the associated damage (Fig. 1b). For instance, the Swiss Forestry Journal published approximate amounts of windfall timber per administrative region (Swiss cantons). A nationwide insurance report (by Lanz-Stauffer and Rommel in 1936)

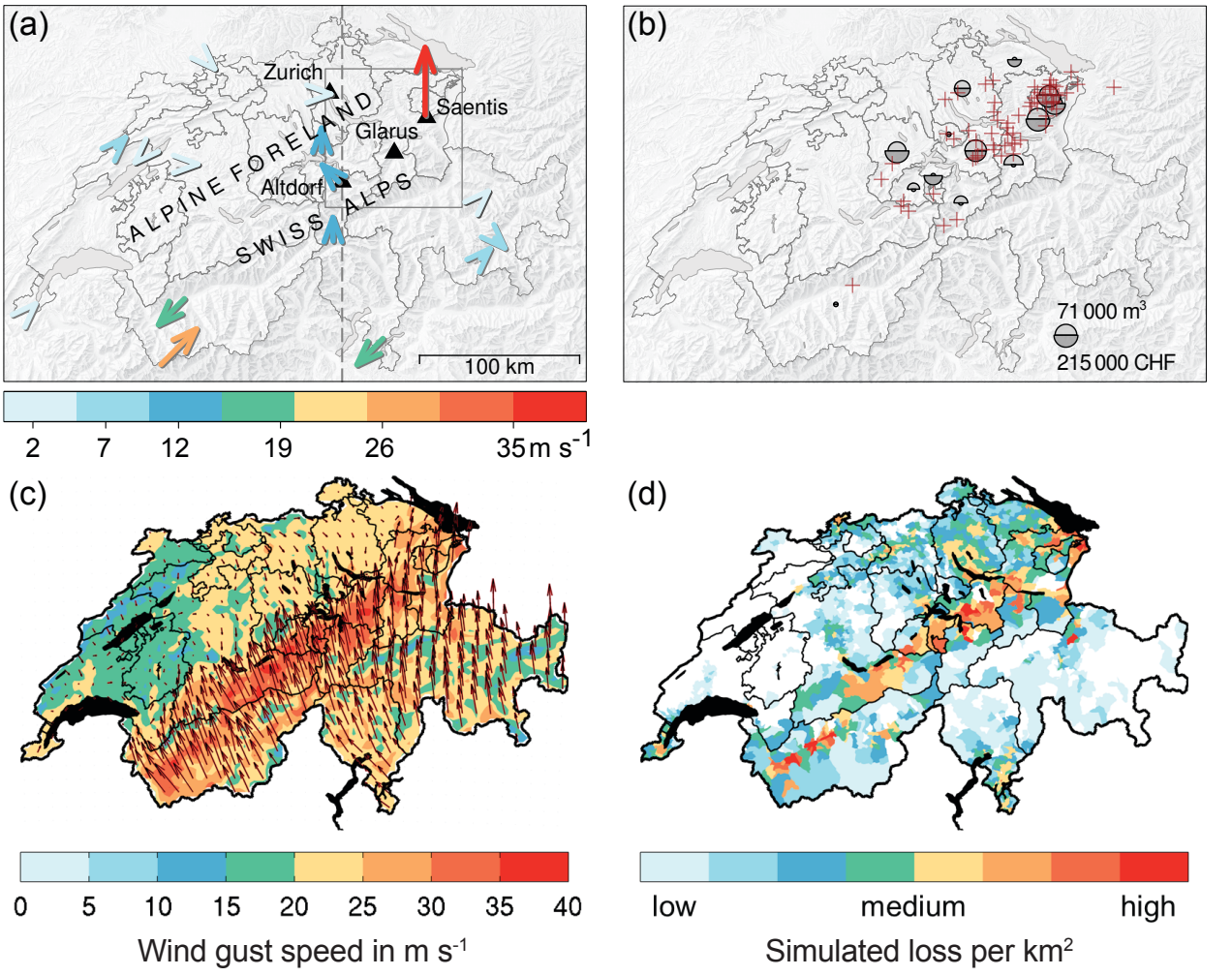


**Fig. 1. (top) Traditional reconstruction vs (bottom) numerical simulation of the (left) wind field and (right) associated damage/loss from the 15 Feb 1925 foehn storm over Switzerland. (a) Manual wind speed observations (colored arrows) at 0600 LT (0500 UTC), converted from half Beauforts. Ticks on the color bar give approximate wind speed in m $s^{-1}$. The color scale is as in (c). Regions and localities (triangles) in Switzerland are as referred to in the text. The dashed line marks the x-axis in Fig. 3b; the box marks the region shown in Fig. 4. The hillshade is courtesy of swisstopo. (b) Reported amounts of windfall timber in cubic meters (light gray segments) and building losses in Swiss francs (dark gray segments) per canton. Red crosses indicate approximate locations of substantial damage as retrieved from newspaper reports. (c) Maximum surface wind gust speed during the historical foehn storm calculated from a weather prediction model at 3-km grid size between 0600 UTC on 13 Feb 1925 and 0800 UTC on 16 Feb 1925 (color shade). The direction of the 10-m instantaneous wind is shown for the time when winds were the most violent in Switzerland (vectors). (d) Simulated monetary loss in Swiss francs per $km^2$ at municipality level under modern (year 2009) socioeconomic conditions related to the historical foehn storm (base-10 logarithmic scale). The monetary loss simulated for each municipality is normalized by the municipal area.**

provided cantonal lists of building losses. Newspapers published dramatic eyewitness reports and roughly located the damage areas—mostly along the Alpine foreland of northeastern Switzerland and at foehn valley exits. Less damage was reported from the foehn valley heads and toward southwestern Switzerland.

Such documentary sources provide important information on the intensities and spatial footprints of historical high-impact windstorms (e.g., Lamb and Frydendahl 1991; Mass and Dotson 2010). These reports are also helpful for weather reconstruction, but need to be complemented with quantitative observations. The

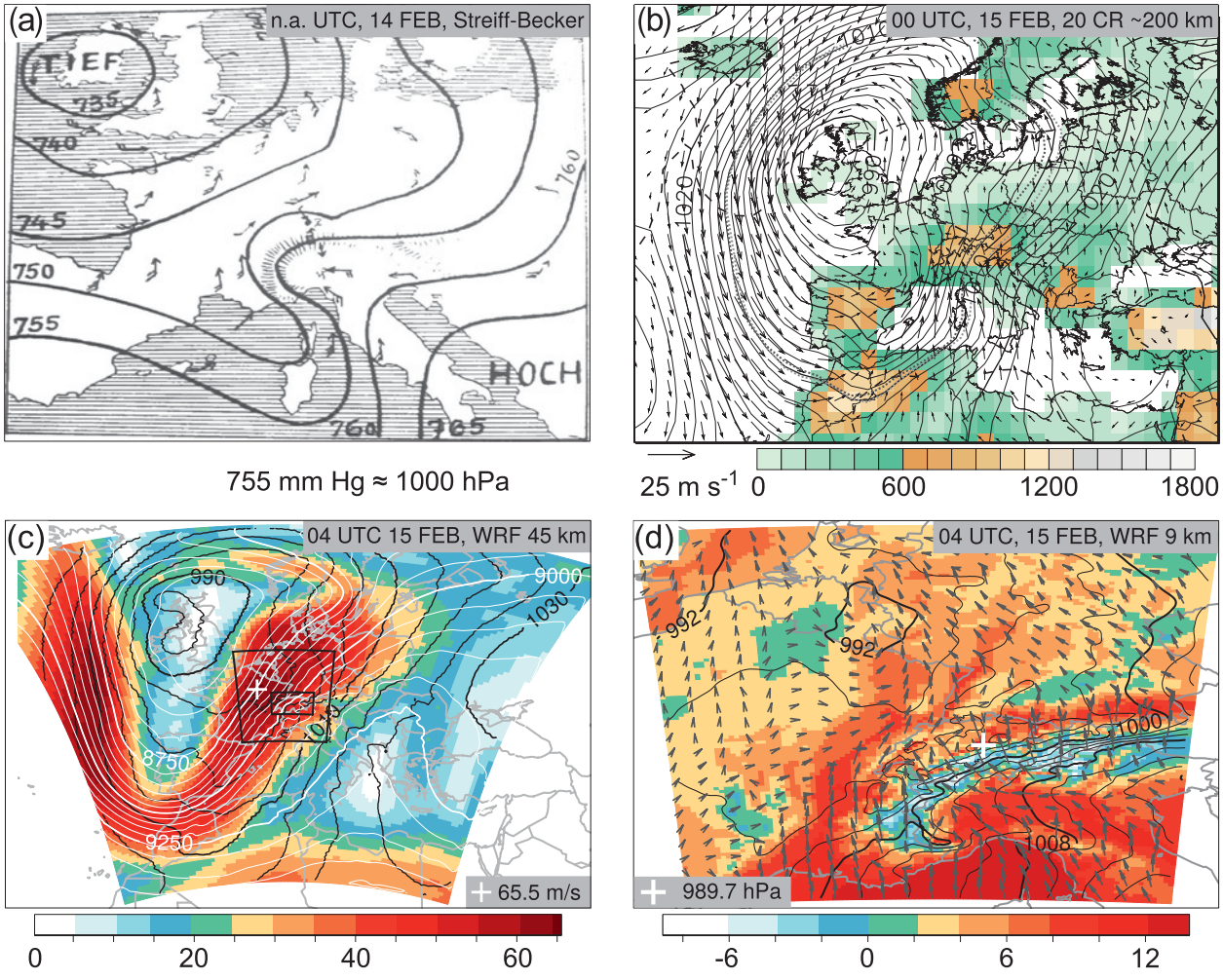


**Fig. 2. (top left) Manual and (top right and bottom panels) numerical meteorological charts of the Feb 1925 foehn storm. (a) Subjective weather chart by Streiff-Becker for 14 Feb 1925 (valid time unknown), adapted from the official weather map by the Swiss Meteorological Institute (today Federal Office of Meteorology and Climatology MeteoSwiss). Surface isobars are in mm Hg (mercury; contours). The Alps (center) are between a depression (*Tief*) over Great Britain and a high (*Hoch*) over southeastern Europe. Surface wind units (1–3 arrow barbs) are unknown. (b) Model topography of the 20CR (m MSL, color shade), 20CR ensemble mean MSLP (hPa, solid contours at 2-hPa intervals), 20CR ensemble spread of MSLP (dashed contour, shown is the 1-hPa deviation, the field maximum is near 1.2 hPa over Central Europe), the 1010 isobars of the ensemble members that produce the strongest (#27, dark gray dotted contour) and weakest (# 51, light gray dotted contour) wind speed over Switzerland, and wind speed at the lowest model level (m $s^{-1}$, black vectors) at 0000 UTC on 15 Feb 1925. (c) Outermost domain of the WRF simulation (45-km grid size) with geopotential height at 300 hPa (m; white contours), wind speed at 300 hPa (m $s^{-1}$, color shade) and MSLP (hPa, black contours at 5-hPa intervals) at 0400 UTC on 15 Feb 1925. Central Europe (9-km domain, black trapezoid) is situated beneath the jet branch with maximum winds (white cross). Switzerland (3-km domain, black rectangle) is located underneath the right exit of the jet. (d) Intermediate domain (9-km grid size) at 0400 UTC on 15 Feb 1925. Shown are air temperature at 2-m height (°C, color shade), MSLP (hPa, black contours at 2-hPa intervals) and 10-m wind vectors (m $s^{-1}$, only every fifth vector in the longitude and latitude direction is plotted). The white cross marks the location of minimum MSLP north of the Alps.**

Swiss Meteorological Institute (today Federal Office of Meteorology and Climatology MeteoSwiss) maintained a relatively small network of wind stations, where manual observations in half Beauforts were recorded three times per day. Figure 1a shows hurricane-force winds on Saentis summit in northeastern Switzerland at 0600

LT (0500 UTC) on 15 February 1925. Gale-force winds were observed in southern to southwestern Switzerland, and strong winds were observed at three stations near Altdorf, all located in a typical foehn valley in central Switzerland. At 1200 LT (1100 UTC), winds increased markedly in Zurich, while weaker winds were observed around Altdorf (not shown).

Meteorologists of the time appreciated the meteorological peculiarities of foehn storms. Scientists had monitored such events since the mid-nineteenth century to establish and corroborate their diverging and sometimes heavily disputed theories of foehn dynamics (Seibert 2012), and Streiff-Becker hence documented the event meticulously. For instance, he drew a surface weather map for Saturday, 14 February 1925 (Fig. 2a). The Alps are situated between a depression over the British Isles and a high over southeastern Europe, and the large pressure gradient across the Alps forms a typical foehn nose. A secondary area of low pressure is located over the western Mediterranean Sea. The associated strong southerly winds turn to easterly approaching the Alps, while southwesterly winds prevail north of the Alps.

In summary, these traditional reconstructions deliver a useful and detailed description of the local wind regimes and damages. However, the hazard and loss information is subjective and incomplete. It does not meet the requirements of modern weather research or risk assessments.

Recently, the 20CR extended the temporal coverage of global atmospheric reanalyses back to 1871, allowing studies of historical weather based on today's numerical and objective methods. The 20CR has proven to be reliable for analyzing synoptic-scale, midlatitude weather systems (Brönnimann et al. 2012; Stucki et al. 2012; Trigo et al. 2014). Going one step further, Michaelis and Lackmann (2013) reconstructed the New England Blizzard of 1888 using the numerical Weather Research and Forecasting model (WRF; Skamarock et al. 2008) to downscale from 20CR input to a 6-km horizontal grid.

**DYNAMICAL DOWNSCALING.** Here, we extend these latest methods with a modeling chain that allows reassessing the high-impact foehn storm of 15 February 1925 on synoptic to mesogamma scales.

The 20CR sets the boundary conditions for the high-resolution downscaling. For this, we use the ensemble mean of the global 56 ensemble member fields,[1] available on a 2° × 2° latitude-longitude grid (grid spacing of approximately 200 km over Central Europe) every 6 h.

In the reanalysis, a deep surface low is located over Great Britain and surface air pressure increases toward southeastern Europe at 0000 UTC on 15 February 1925 (Fig. 2b). Mean sea level pressure (MSLP) differences across the Alps are approximately 5.5 hPa (20CR ensemble range 3–6.5 hPa, not shown). A very strong southerly flow extends from the Sahara to the Alps, but wind speeds north of the Alps are rather low. It is evident that the 20CR can resolve the large-scale flow, but the foehn nose and the potential area of low pressure over the Mediterranean in Fig. 2a are not accentuated in the 20CR. The 2-degree grid of the 20CR is too coarse to realistically represent the complex topography of the Alps, and hence fails to capture wind systems that are strongly influenced by this factor.

To compensate, we employ dynamical downscaling for a closer look at the Alpine region. 20CR ensemble mean fields (and the 20CR ensemble members #27 and #51, see Footnote 1) provide the initial and lateral boundary conditions that drive the regional, higher-resolution WRF model (version 3.3.1) for a limited domain over Europe. Two more refinement steps result in three domains. Horizontal grid spacing decreases from 45 km in the largest domain to 9 km in the intermediate to 3 km in the smallest domain, which covers Switzerland and adjacent regions. The vertical structure of the atmosphere is described using 31 vertical layers.[2] Hourly model output is used for the analysis. The simulation starts at 0600 UTC

[1] During the foehn storm, the 20CR ensemble standard deviation of mean sea level pressure (MSLP) remains small over Europe (≤1.2 hPa; cf. Fig. 2b), indicating a small range of probable initial conditions. Over most of the same period, the two members related to the highest (#27) and lowest (#51) wind speeds over Switzerland differ by 0.5–1.5 hPa in the MSLP field (not shown). At 0000 UTC on 15 February 1925, the ensemble mean and member #27 produce similar pressure gradients across the Alps (5.5 hPa and 6 hPa), whereas #51 is an outlier, concomitant with the lowest pressure gradient across the Alps (3 hPa, Fig. 2b). Accordingly, selected information from the downscaled members #27 and #51 provides evidence of a more probable versus an outlier simulation over the core period of the foehn storm (see text).

[2] Turbulence is calculated by using the Mellor-Yamada scheme and the surface layer is parameterized according to the Monin-Obukhov scheme. The microphysics scheme by Lin et al. (1983) is used together with the RRTM scheme for longwave and the Dudhia scheme for shortwave radiation.

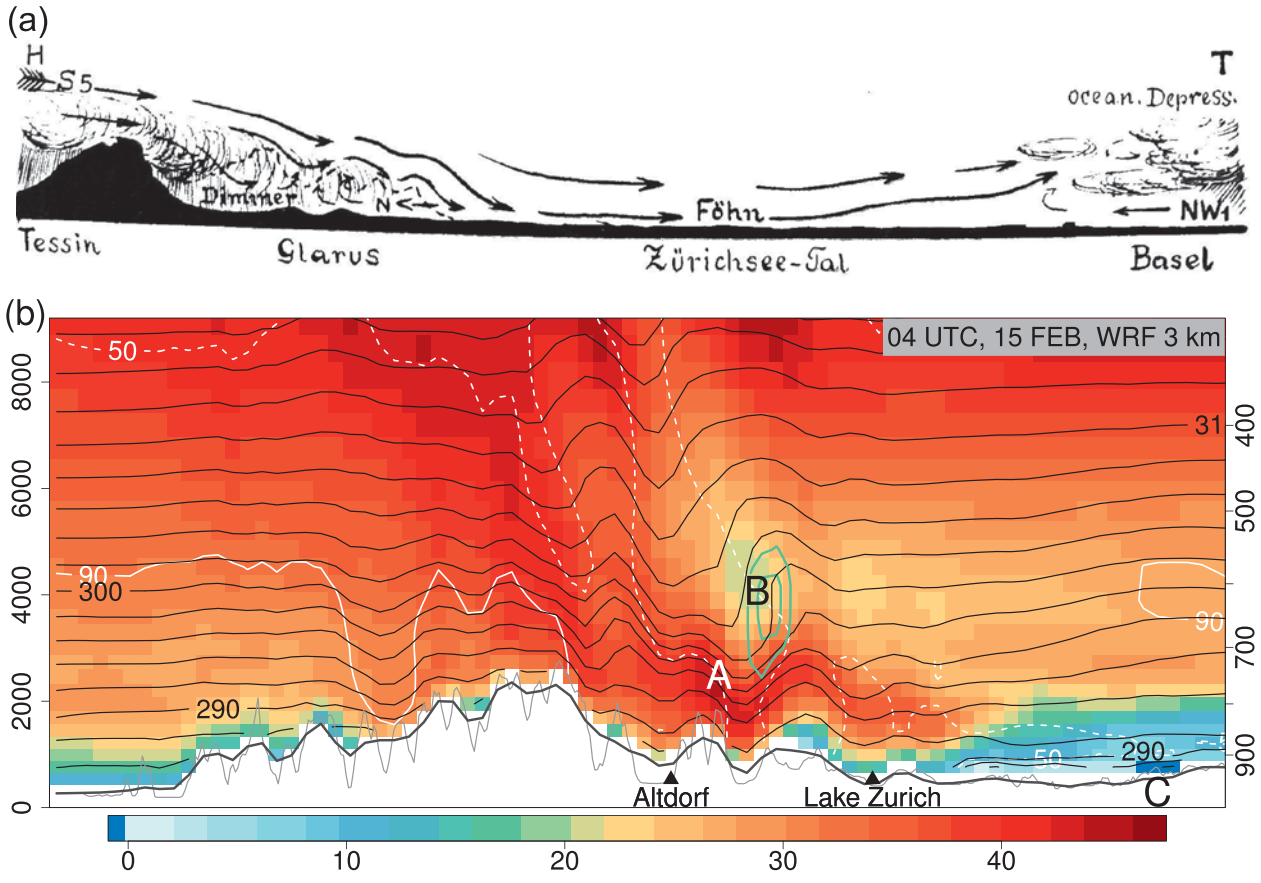


**Fig. 3. (top) Conceptual and (bottom) numerical vertical cross sections across the Alps on 15 Feb 1925 (two parallel valleys). (a) Cross section from south to north through canton of Glarus and across Lake Zurich (*Zürichseetal*) by Streiff-Becker. High pressure (*H*) is located on the south side of the Alps, lower pressure (T) toward the oceanic depression northwest of Switzerland. The southerly flow on the mountain tops reaches 5 half Beauforts (approx. 25 m $s^{-1}$), the shallow counter-flow from northwest 1 half Beaufort (approx. 1.6 m $s^{-1}$). Heavy precipitation is depicted on the upwind side of the Alpine range, and wind-dragged clouds with drizzle cause dimmed daylight (*Dimmer*) near Glarus. Turbulent and very strong foehn winds touch ground near Lake Zurich. (b) Cross section from south to north, through Altdorf and Lake Zurich (dashed line in Fig. 1a) at 0400 UTC on 15 Feb 1925. Height is given in m MSL (left y-axis) and in hPa (right y-axis). WRF model terrain (thick gray line) is compared to a topography model (thin gray line, obtained from Google Elevation API); the locations of Altdorf and Lake Zurich are marked with triangles. South-north wind speed components (m $s^{-1}$, color shade, reverse flow in dark blue), potential temperature (K, black contours), a lower-tropospheric region of enhanced turbulent kinetic energy (1 $m^2$ $s^{-2}$ and 3 $m^2$ $s^{-2}$, outer and inner pale green contours), and relative humidity (50 and 90%; dashed and solid white contours) are indicated. Label A marks the region with strongest low-level winds, label B an area of increased instability and reduced wind, and label C a shallow layer with reverse flow.**

on 13 February 1925 (the lead time of >1 day allows small-scale atmospheric features to spin up) and ends at 0800 UTC on 16 February 1925.

## HIGH-RESOLUTION NUMERICAL SIMULATION: METEOROLOGY REVISITED.

Next, we analyze the main meteorological features in the 45-km WRF domain at 0400 UTC on 15 February 1925 (Fig. 2c). Reportedly, this is the time when the first intense foehn phase occurred. At the 300-hPa level, there is an elongated trough over Western Europe, and wind speeds of up to 65 m $s^{-1}$ in the downscaled ensemble mean (denoted DEM hereafter; 65 m $s^{-1}$ in member #27, 60 m $s^{-1}$ in #51, not shown) indicate the presence of the jet stream over Central Europe. The Alps are on the anticyclonic

side of the jet maximum. In the right-front quadrant of the jet, subsidence increases the stability aloft, and this in turn supports the strengthening of downslope winds at the surface (Jackson et al. 2013; COMET 2014).

At the same time, topographically induced modulations of the surface pressure field become gradually more apparent in the 45-km and 9-km domains (Figs. 2c and 2d), and typical mesoscale foehn features emerge. In Fig. 2d, MSLP contours delineate the foehn nose, and minimum MSLP values near 990 hPa are found in the foehn regions, which results in a pressure difference of approximately 16 hPa in the DEM (14 hPa in #27, 6 hPa in #51) across the Alps. This agrees well with a difference of 12 hPa between Basel (northern Switzerland) and Lugano (southern Switzerland; reported in the Annals of the Swiss Meteorological Institute), and with Streiff-Becker's weather chart (Fig. 2a). As in the 20CR, the secondary area of low pressure over the central Mediterranean is not very accentuated. For 1925, MSLP assimilation in the 20CR is based on a relatively dense network in the Mediterranean area (see ISPD 2014) and the 20CR ensemble standard deviation is small (≤1.2 hPa, c.f. Fig. 2b). In Fig. 2a, the wind vectors south of France are rather inconsistent with the pressure field, but in agreement with the 20CR and the WRF output (Figs. 2b–d). This points to the lobe over the Mediterranean in Streiff-Becker's conceptual chart being exaggerated. Except for this region and a secondary low over Belgium, the downscaled surface wind field (Fig. 2d) agrees well with the historic weather chart, and strong surface winds prevail across the Alps. Warm spots of around 15°C in the DEM (15°C in #27, 8°C in #51, not shown) are found along the north side of the Alps (Fig. 2d). This corresponds with reports of 17°C on higher grounds in the foehn regions at 0700 LT (0600 UTC).

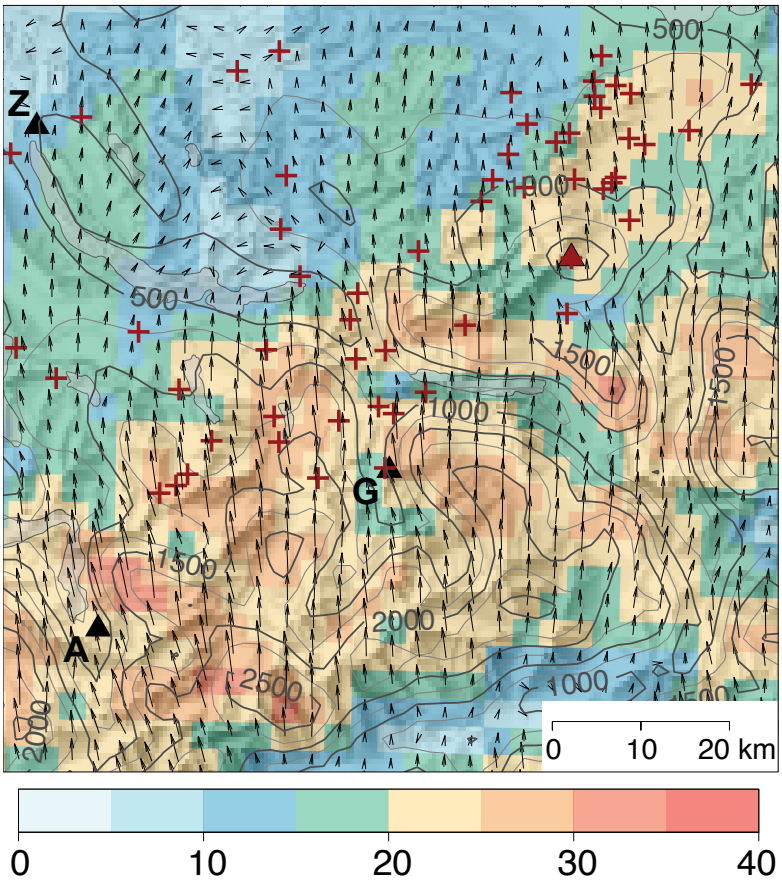


**Fig. 4. Maximum 10-m wind speed (m s$^{-1}$, color shade) and wind direction at 3-km horizontal grid-spacing (black arrows) during the foehn storm period (13–16 Feb 1925) at the time of maximum wind speed over northeastern Switzerland (see inset in Fig. 1a). Model terrain contours (m MSL, dark gray and gray lines) are plotted over the background hillshade (courtesy of swisstopo). Locations of Saentis summit (2,502 m MSL, dark red triangle), Zurich (label Z), Glarus (label G), and Altdorf (label A) are marked (c.f. Fig. 1a). Dark red crosses are locations of substantial damage (as in Fig. 1b).**

Streiff-Becker's conceptual cross section of the wind field through Glarus on 15 February 1925 shows further interesting features of the foehn storm (Fig. 3a). A very strong southerly flow (25–35 m s$^{-1}$) advects precipitating clouds across the Alps, causing so-called *dimmer* (dimmed daylight) in the Glarus valley. Here, surface winds can be turbulent, and even weak northerlies are observed. The actual, very strong foehn winds touch the surface farther north in the Alpine forelands near Lake Zurich. Farther downstream, they are lifted over a shallow layer of colder air, wherein a weak reverse flow persists.

A similar perspective emerges from the high-resolution simulations (Fig. 3b) for 0400 UTC on 15 February 1925. Shown is a south-north cross-section through the 3-km model domain (i.e., across the Alpine divide and through Altdorf). This section is parallel to Fig. 3a; it was chosen because the topography is closer to single-range mountains used in idealized flow simulations than at Glarus.

Decreasing spacing of the isentropes between the surface and the midtroposphere indicates increasing atmospheric stability on the upwind side of the mountain top (lapse rates of 5–6°C $km^{-1}$, not shown). The cross-barrier flow is very strong in the DEM (≥30 m $s^{-1}$; ≥28 m $s^{-1}$ in #27, ≥20 m $s^{-1}$ in #51, not shown), and wind speed generally increases with height. Relative humidity at lower levels exceeds 90% (Fig. 3b). This is a "textbook" deep foehn situation with forced moist-adiabatic ascent of air and associated heavy precipitation on the southern side of the Swiss Alps (Richner and Hächler 2013).

Downwind of the mountain barrier, relative humidity decreases rapidly, indicating the foehn wall and subsequent clear sky. The changing atmospheric stability and the complex terrain produce a flow with many typical features of a mountain wave (Markowski and Richardson 2010; Jackson et al. 2013; Richner and Hächler 2013; COMET 2014). Tightly spaced, downward-sloping isentropes follow a tongue of very strong low-level winds in the DEM (>40 m $s^{-1}$, label A in Fig. 3b; >40 m $s^{-1}$ in # 27, no comparable feature in # 51, not shown). Above the abrupt upward deflection of the flow, there is an area with unstable stratification (delineated by vertical isentropes), enhanced turbulent kinetic energy (>3 $m^2$ $s^{-2}$ in the DEM; >2 $m^2$ $s^{-2}$ in #27, no comparable feature in # 51, not shown), and reduced cross-barrier wind speeds (label B). This indicates a potential critical layer and possible gravity-wave breaking. Critical layers can inhibit upward energy propagation, increase the downward wind component, and thus support wind acceleration and turbulence beneath. Hence, strongest surface winds are expected below this area (i.e., between Altdorf and Lake Zurich). Note also the shallow reverse flow over northern Switzerland (label C).

A high-resolution map (Fig. 4, a section of the 3-km domain) provides a comparison of the strongest modeled winds during the foehn storm with approximate damage locations at a mesogamma scale. Very strong surface winds (≥20 m $s^{-1}$ in the DEM; gradually weaker in #27 and #51, not shown) are found along the northern flanks of the Alpine range, and particularly at the exit of the Glarus valley (label G). These high-wind areas correspond to the areas where most of the reported damages occurred. This provides evidence that the WRF model is able to simulate small-scale effects like the northward shift of the foehn touchdown in the Glarus valley.

However, some limitations of the downscaling also become apparent at this spatial scale. One limitation is that the topography in the WRF model is too smooth (see also Fig. 3). As a consequence, the modeled airflow tends to tightly follow the downwind mountain slopes. In reality, we expect that the airflow decoupled more effectively from the steep, north-side mountain flanks and the region of abrupt flow uplift was shifted a little farther to the north, away from the mountains in some areas. This could partly explain the moderate simulated winds over a few damage areas located some distance from the Alpine range (Fig. 4). Another limitation is that some of the damage is probably due to channeling and turbulence effects that cannot be resolved at a 3-km grid size. The reported intense foehn phases are generally reproduced with a lag of ±1–3 h in the DEM (same lags in #27 and #51), but the simulation does not clearly indicate that the winds were stronger (weaker) at Zurich (Glarus) at noon compared to the early morning hours (not shown). Last, the foehn event probably set in too early, and ended too late in the simulations (not shown, cf. Richner and Hächler 2013).

In summary, the documentary reconstruction is qualitatively consistent with our numerical simulations. Some of the regional and very local characteristics of this so-called *dimmer-foehn* event are only identifiable in the model data (e.g., deep trough extending into the Sahara and associated synoptic circulation, foehn lows at mesogamma scale, low- to midtropospheric mountain wave patterns), while other foehn features seem more plausible from conceptual thinking or from the observations (e.g., *dimmer*, weak northerly flow near Altdorf and Glarus around noon).

**LOSS SIMULATION: HISTORICAL STORM OVER MODERN LANDSCAPES.** The generally accurate and dynamically consistent wind fields from WRF output provide an encouraging basis for modeling the storm-related losses. High damage is typically related to maximum wind gusts (e.g., Klawa and Ulbrich 2003). Therefore, wind gust speeds from standard WRF postprocessing were used for impact modeling instead of the instantaneous wind speed values considered so far; the latter correspond approximately to 10-min values. With our approach, we model the potential economic losses from the 15 February 1925 foehn storm using present-day asset distributions in Switzerland. The economic losses are estimated at the municipality level, based on the field of the maximum downscaled surface wind gust speeds over Switzerland during the event (Fig. 1c)

and the probabilistic damage assessment module of the climate adaptation model (climada[3]; Bresch 2014; Reguero et al. 2014). In the climada model, we prescribe a modern (i.e., 2009) population distribution, assuming assets of 250,000 Swiss francs per inhabitant. For each municipality, the monetary damage is simulated based on the product between the respective asset value and a nonlinear damage function. This function (derived by Schwierz et al. 2010) relates the damage of a particular asset to the incurring wind gust at this location.

The model simulates high losses in northeastern Switzerland as well as in some regions of the Alps (Fig. 1d), where the wind gusts reach high values (Fig. 1c). In addition, metropolitan areas are recognizable in Fig. 1d, indicating that simulated storm losses are related to the distribution of both asset values and hazardous wind speeds.

In general, the pattern of simulated losses corresponds well with the pattern of reported losses associated with the foehn storm (Fig. 1b; slightly to moderately lower damage using #27 and #51, not shown). In particular, the damage locations between Altdorf and Glarus, around Lake Zurich and Saentis, are very well reproduced in the simulation, and even some damage areas in the Alpine foreland are well collocated with the reconstruction. However, we have very few to no damage reports from some areas with simulated losses, such that metropolitan areas are possibly overrepresented in the damage pattern. Such discrepancies could partly be due to nonreporting of losses from more remote areas (e.g., from southwestern Switzerland). Indeed, catastrophic precipitation and avalanches in southern Switzerland dominated the news from this region. Furthermore, we prescribed today's distribution of asset values in Switzerland in the climada loss model. These values have changed considerably since 1925.

A further limitation may come from modeling losses at the municipality level: wind gust speeds, which are usually high on mountain tops, are combined with assets, which are typically high at valley bottoms.

[3] Climada is the open-source version of the Swiss Re operational natural catastrophe loss model, and provides an assessment of risk from natural hazards such as extratropical windstorms or tropical cyclones. A precursor was used to model losses from European winter storms in current and future climate (Schwierz et al. 2010).

**LESSONS FROM THE EXPLORATORY ANALYSIS.** We have shown that the downscaling and loss modeling chain enables the numerical, local-scale simulation of an extreme windstorm in the early twentieth century, and hence enables assessing potential harm from historical natural hazards in today's (and possibly a future) world.

WRF-downscaling of the 20CR produces realistic wind fields on smaller scales and over complex terrain, although there are limitations regarding the exact location, intensity, and timing of the wind maxima. Our analyses of the 20CR ensemble mean, the 20CR ensemble members, and the three WRF simulations (DEM, #27, and #51) indicate that the 20CR ensemble mean and the DEM are suitable estimates of the initial and local-scale atmospheric conditions for this historical foehn storm. Nevertheless, our WRF simulations represent only three possible realizations of a very complex event, and there remain many opportunities to improve the simulation configuration. For instance, using all 56 ensemble members of the 20CR could provide an uncertainty estimation of our findings. Additionally, different gust parameterization schemes or a further spatial refinement of the simulations to a few hundred meters grid size and with an increased number of vertical levels should be tested in future work. The climada model output reflects the spatial distribution of reported impacts satisfactorily. However, refining the damage function in the model is necessary for more quantitative analyses.

We have also shown that historical expert concepts, reports, and sparse observations still remain valid and are very valuable sources for weather and impact reconstruction. We therefore advocate a complimentary use of both traditional and numerical techniques.

Besides detailed case studies of historical events, our approach facilitates statistical or dynamical analyses of meaningful sample sizes (e.g., of extreme impacts at centennial time scales). It may break new ground for applications that require high-resolution, consistent, and long-term data coverage. In this sense, these novel opportunities for numerical simulations may well change our perspectives on historical high-impact weather.

## FOR FURTHER READING

American Meteorological Society, cited 2014: Foehn. *Glossary of Meteorology*. [Available online at http://glossary.ametsoc.org/wiki/Foehn.]

Bresch, D. N., 2014: climada. [Available online at https://github.com/davidnbresch/climada; winter storm module at https://github.com/davidnbresch/climada_module_ws_europe; introduction at www.iac.ethz.ch/edu/courses/master/modules/climate_risk/2013.]

Brönnimann, S., O. Martius, H. von Waldow, C. Welker, J. Luterbacher, G. P. Compo, P. D. Sardeshmukh, and T. Usbeck, 2012: Extreme winds at northern mid-latitudes since 1871. *Meteorol. Z.,* **21,** 13–27, doi:10.1127/0941-2948/2012/0337.

COMET, cited 2014: Mountain waves and downslope winds. [Available online at www.meted.ucar.edu/mesoprim/mtnwave/.]

Compo, G. P., and Coauthors, 2011: The Twentieth Century Reanalysis Project. *Quart. J. Roy. Meteor. Soc.,* **137,** 1–28, doi:10.1002/qj.776.

ISPD, cited 2014: The International Surface Pressure Databank. [Available online at www.esrl.noaa.gov/psd/data/ISPD/.]

Jackson, P. L., G. Mayr, and S. Vosper, 2013: Dynamically-driven winds. *Mountain Weather Research and Forecasting: Recent Progress and Current Challenges,* F. K. Chow, S. F. J. De Wekker, and B. J. Snyder, Eds., Springer, 121–218.

Klawa, M., and U. Ulbrich, 2003: A model for the estimation of storm losses and the identification of severe winter storms in Germany. *Nat. Hazards Earth Syst. Sci.,* **3,** 725–732, doi:10.5194/nhess-3-725-2003.

Lamb, H., and K. Frydendahl, 1991: *Historic storms of the North Sea, British Isles, and Northwest Europe.* Cambridge University Press, 228 pp.

Lanz-Stauffer, H., and C. Rommel, 1936: Elementarschäden und Versicherung: Studie des Rückversicherungsverbandes kantonal-schweizerischer Feuerversicherungsanstalten zur Förderung der Elementarschadenversicherung. Im Selbstverlag des Rückversicherungsverbandes.

Lin, Y.-L., R. D. Farley, and H. D. Orville, 1983: Bulk parameterization of the snow field in a cloud model. *J. Climate Appl. Meteor.,* **22,** 1065–1092.

Markowski, P., and Y. P. Richardson, 2010: *Mesoscale Meteorology in Midlatitudes.* Wiley-Blackwell, 430 pp.

Mass, C., and B. Dotson, 2010: Major extratropical cyclones of the northwest United States: Historical review, climatology, and synoptic environment. *Mon. Wea. Rev.,* **138,** 2499–2527, doi:10.1175/2010MWR3213.1.

Michaelis, A. C., and G. M. Lackmann, 2013: Numerical modeling of a historic storm: Simulating the Blizzard of 1888. *Geophys. Res. Lett.,* **40,** 4092–4097, doi:10.1002/grl.50750.

Reguero, B. G., D. N. Bresch, M. W. Beck, J. Calil, and I. Meliane, 2014: Coastal risks, nature-based defenses and the economics of adaptation: An application in the Gulf of Mexico, USA. *Coastal Engineering Proc.,* 1–15.

Richner, H., and P. Hächler, 2013: Understanding and Forecasting Alpine Foehn. *Mountain Weather Research and Forecasting: Recent Progress and Current Challenges,* F. K. Chow, S. F. J. De Wekker, and B. J. Snyder, Eds., Springer, 219–260.

Schwierz, C., P. Köllner-Heck, E. Zenklusen Mutter, D. N. Bresch, P.-L. Vidale, M. Wild, and C. Schär, 2010: Modelling European winter wind storm losses in current and future climate. *Climatic Change,* **101,** 485–514, doi:10.1007/s10584-009-9712-1.

Seibert, P., 2012: The riddles of foehn—introduction to the historic articles by Hann and Ficker. *Meteor. Z.,* **21,** 607–614, doi:10.1127/0941-2948/2012/0398.

Skamarock, W. C., J. B. Klemp, D. O. Gill, D. M. Barker, M. G. Duda, W. Wang, and J. G. Powers, 2008: A description of the advanced research WRF version 3. NCAR Tech. Note NCAR/TN-475+STR, 113 pp, doi:10.5065/D68S4MVH.

Stucki, P., R. Rickli, S. Brönnimann, O. Martius, H. Wanner, D. Grebner, and J. Luterbacher, 2012: Weather patterns and hydro-climatological precursors of extreme floods in Switzerland since 1868. *Meteor. Z.,* **21,** 531–550, doi:10.1127/0941-2948/2012/368.

——, S. Brönnimann, O. Martius, C. Welker, M. Imhof, N. von Wattenwyl, and N. Philipp, 2014: A catalog of high-impact windstorms in Switzerland since 1859. *Nat. Hazards Earth Syst. Sci.,* **14,** 2867–2882, doi:10.5194/nhess-14-2867-2014.

Trigo, R. M., F. Varino, A. M. Ramos, M. A. Valente, J. L. Zêzere, J. M. Vaquero, C. M. Gouveia, and A. Russo, 2014: The record precipitation and flood event in Iberia in December 1876: Description and synoptic analysis. *Front. Earth Sci.,* **2,** doi:10.3389/feart.2014.00003.

# AMS MEMBERS

# GIVE A GREAT GIFT AT A GREAT PRICE

Looking for the perfect present for the weather enthusiast in your life? Want to make a valuable contribution to your local library or community college? Send a subscription to *Weatherwise* magazine (calendar year) for just $24.95*—That's nearly 50% off the list price!

Written for a general audience, *Weatherwise* offers a colorful and nontechnical look at recent discoveries in meteorology and climatology. Check out the latest table of contents at www.weatherwise.org.

Want your own? Then order a personal subscription at the same great price.


Contact Member Services by e-mail at amsmem@ametsoc.org or by phone at 617-227-2425 to place all of your *Weatherwise* orders today!

*Cost for delivery outside of the U.S. is $40.95. *Weatherwise* is available to AMS Members through a cooperative agreement with Taylor & Francis Group LLC, the publishers of *Weatherwise*.